The Astrophysical Journal, 692:L96–L99, 2009 February 20 doi:10.1088/0004-637X/692/2/L96

SPECTROSCOPIC EVIDENCE FOR GAS INFALL IN GF 9-2

Ray S. Furuya[1], Yoshimi Kitamura[2], and Hiroko Shinnaga[3]
[1] Subaru Telescope, National Astronomical Observatory of Japan, 650 North A'ohoku Place, Hilo, HI 96720, USA; rsf@subaru.naoj.org
[2] Institute of Space and Astronautical Science, Japan Aerospace Exploration Agency, 3-1-1 Yoshinodai, Sagamihara, Kanagawa 229-8510, Japan; kitamura@isas.jaxa.jp
[3] Caltech Submillimeter Observatory, California Institute of Technology, 111 Nowelo Street, Hilo, HI 96720, USA; shinnaga@submm.caltech.edu
Received 2008 September 13; accepted 2009 January 6; published 2009 February 3

ABSTRACT

We present spectroscopic evidence for the infall motion of gas in the natal cloud core harboring an extremely young low-mass protostar GF 9-2. We previously discussed that the ongoing collapse of the GF 9-2 core has agreement with the Larson–Penston–Hunter (LPH) theoretical solution for the gravitational collapse of a core. To discuss the gas infall on firmer ground, we have carried out on-the-fly mapping observations of the HCO^+ (1–0) line using the Nobeyama 45 m telescope equipped with the 25 Beam Array Receiver System. Furthermore, we observed the HCN (1–0) line with the 45 m telescope, and the HCO^+ (3–2) line with the Caltech Submillimeter Observatory 10.4 m telescope. The optically thick HCO^+ and HCN lines show blueskewed profiles whose deepest absorptions are seen at the peak velocity of optically thin lines, i.e., the systemic velocity of the cloud, indicating the presence of gas infall toward the central protostar. We compared the observed HCO^+ line profiles with model ones by solving the radiative transfer in the core under LTE assumption. We found that the core gas has a constant infall velocity of $\sim$0.5 km s^{-1} in the central region, leading to a mass accretion rate of $2.5\times10^{-5}\,M_\odot$ yr^{-1}. Consequently, we confirm that the gas infall in the GF 9-2 core is consistent with the LPH solution.

Key words: ISM: clouds – ISM: evolution – ISM: individual (GF 9-2, L 1082) – ISM: molecules – stars: formation – stars: pre-main sequence

1. INTRODUCTION

Without accurate knowledge of the collapsing process of an isolated dense cloud core, we cannot understand how a low-mass protostar forms through the accretion process. One of the major limiting factors is that the initial conditions of core collapse are not necessarily revealed by observations in detail. There has been a long-standing theoretical debate about the gravitational collapse process since the early 1970s. Two extreme models of runaway collapse and quasi-static, inside-out collapse have been developed; the former was originally proposed by Larson (1969) and Penston (1969) and extended by Hunter (1977), and the latter by Shu (1977). In this Letter, we refer to the runaway collapse scenario as the Larson–Penston–Hunter (LPH) solution following the nomenclature in McKee & Ostriker (2007). The validity of these solutions has been observationally studied by, e.g., Ward-Thompson et al. (1994) and Looney et al. (2003).

In this context, we performed a detailed study of the natal cloud core harboring an extremely young low-mass protostar GF 9-2 (Furuya et al. 2006; hereafter Paper I). The protostar is believed not to have generated an extensive molecular outflow, yielding a rare opportunity to investigate core collapse conditions free from the disturbance by the outflow. We discussed that the observed velocity field of the core is consistent with the initial conditions assumed in the LPH solution. The core shows a radial density profile $\rho(r) \propto r^{-2}$ and the entire core has nonthermal line widths of $\Delta v_{\rm nth} \sim$ (2–3)$c_{\rm iso}$, suggestive of gas infall motions ($c_{\rm iso}$ is isothermal sound velocity). In order to shed light on the physical properties of the infall motions, we have carried out molecular line observations of the GF 9-2 core to detect the blueskewed profiles characterizing infall motion (e.g., Walker et al. 1986; Zhou et al. 1993; Ward-Thompson et al. 1996; Myers et al. 1996; Mardones et al. 1997; Onishi et al. 1999; Remijan & Hollis 2006).

2. OBSERVATIONS

We have carried out on-the-fly (OTF) mapping observations (Sawada et al. 2008) of the HCO^+ J =1–0 line (rest frequency ($\nu_{\rm rest}$) = 89188.526 MHz) using the Nobeyama Radio Observatory (NRO)[4] 45 m telescope in 2007 May. We used the 25 Beam Array Receiver System (BEARS), and configured autocorrelators (ACs) as a backend, yielding an effective velocity resolution ($\Delta v_{\rm res}$) of 0.048 km s^{-1} in the 8 MHz bandwidth mode. At the line frequency, the mean beam size ($\theta_{\rm HPBW}$) of the 25 beams was 18.″6, and the mean main-beam efficiency ($\eta_{\rm mb}$) was 0.51. All the spectra were calibrated by the standard chopper wheel method, and were converted into main-beam brightness temperature ($T_{\rm mb}$) by dividing by $\eta_{\rm mb}$. We adopted the correction factors provided by the observatory for gain differences between the 25 beams. The uncertainty in our intensity calibration is estimated to be $\sim$ 15%. The OTF mapping was carried out over an area with a size of $\sim$320″, employing the position switching method. The telescope pointing was checked every 1.2 hr, and was found to be accurate within 3″. The data reduction was done using the NOSTAR package. By using a spheroidal function as a gridding convolution function, we produced a data cube with a spatial resolution of 20.″6 and a pixel size of 5″. Furthermore, in 2008 June, we performed a single-point integration of the HCN (1–0) line toward the core center with the 45 m telescope. The beam size of the S80 receiver at the line frequency was 18.″2 in HPBW, and $\eta_{\rm mb}$ was 0.44. We used acousto-optical spectrometers (AOSs), AOS-H, providing $\Delta v_{\rm res}$ of 0.13 km s^{-1}.

In 2006 July, 2007 August, and 2008 June, we used the Caltech Submillimeter Observatory (CSO)[5] 10.4 m tele-

[4] The Nobeyama Radio Observatory is a branch of the National Astronomical Observatory of Japan, National Institutes of Natural Sciences.
[5] The Caltech Submillimeter Observatory is operated by the California Institute of Technology under the grant from the US National Science Foundation (AST 05-40882).

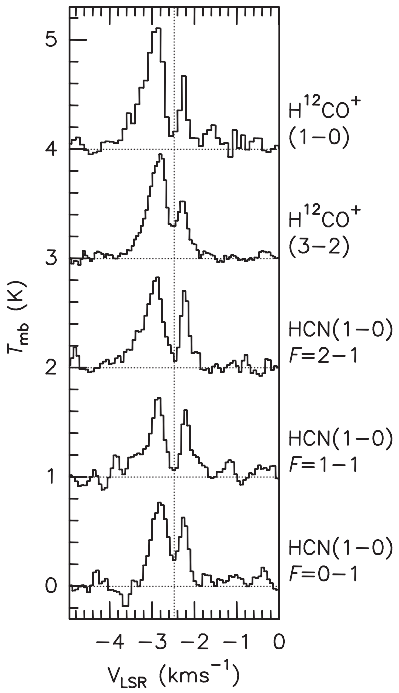

Figure 1. Single-dish spectra of the molecular line emission toward the GF 9-2 core center shown in the main-beam brightness temperature (T_{mb}) scale. The HCO^+ (1–0) spectrum is smoothed so as to have the effective resolution of 26″ in FWHM, i.e., the CSO beam size for the HCO^+ (3–2) line. The rms noise levels are 73 mK, 61 mK, and 88 mK for the HCO^+ (1–0), HCO^+ (3–2), and the HCN lines, respectively. To convert the rest frequency (ν_{rest}) of the HCN HF emission to the LSR velocity (V_{LSR}), we adopted the systemic velocity (V_{sys}) of −2.48 km s^{-1} (Paper I), and ν_{rest} = 88630.41406 MHz for F = 1–1, 88631.84375 MHz for F = 2–1, and 88633.93750 MHz for F = 0–1. The vertical dashed line shows the systemic velocity of the cloud, V_{sys} = −2.48 km s^{-1} (Paper I).

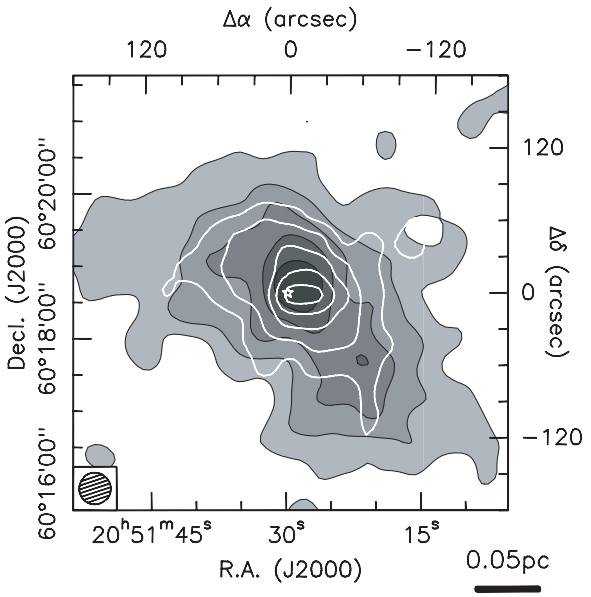

Figure 2. Overlay of the total integrated intensity maps of the $H^{13}CO^+$ (1–0) emission (white contour; Paper I) on that of the HCO^+ (1–0) emission (gray-scale with thin contour; this work) emission. The contour levels for the HCO^+ emission have the 3σ intervals starting from the 3σ level where σ = 0.59 K km s^{-1}. The HCO^+ emission is integrated over an LSR velocity range between −3.60 km s^{-1} and −1.95 km s^{-1}. The central star marks the peak position of the 3 mm continuum emission (Paper I). The hatched circle at the bottom left corner indicates the effective beam size of the HCO^+ emission, which is set to be equal to the CSO beam size for HCO^+ (3–2) (θ_{HPBW} = 26″; see Section 2).

scope to observe the HCO^+ J = 3–2 transition (ν_{rest} = 267557.633 MHz). We assumed θ_{HPBW}= 26″ at 267 GHz and estimated η_{mb} of 0.70 ± 0.15 from our measurements of Jupiter. We configured the 50 MHz bandwidth AOS, providing Δv_{res} of 0.055 km s^{-1}. The HCO^+ line was observed toward 3×3 positions with a grid spacing of 30″ centered on the GF 9-2 core center. The pointing accuracy was better than 3″, and the overall uncertainty in flux calibration was 30%.

3. RESULTS

Figure 1 shows molecular line spectra toward the GF 9-2 core center in units of T_{mb}. All the spectra, except the HCO^+ J = 1–0, are the single-dish spectra taken with position switching. The HCO^+ (1–0) spectrum was produced from the data cube (Section 2) by convolving with a Gaussian profile in order to have an effective spatial resolution of 26″ in FWHM, which is equal to the CSO beam size for the HCO^+ (3–2) line. Clearly, all the spectra show blueskewed profiles. The LSR velocities of their deepest absorption agree with the systemic velocity (V_{sys}) of the cloud, V_{LSR}= −2.48 km s^{-1}, which was estimated from the optically thin $H^{13}CO^+$ (1–0) and CCS $4_3 - 3_2$ lines (Paper I) as well as NH_3 inversion lines at 23 GHz (Furuya et al. 2008).

The velocities of the blueshifted peaks of the HCO^+ (1–0) and (3–2) lines, $V_{p,blue}$ are estimated to be −2.96 ± 0.02 km s^{-1} and −2.86 ± 0.01 km s^{-1}, respectively, from Gaussian fitting. Similarly, we obtained $V_{p,red}$ = −2.29 ± 0.01 km s^{-1} and −2.25 ± 0.05 km s^{-1} for the redshifted peaks of the (1–0) and (3–2) transitions, respectively. The obtained $V_{p,red}$ for both the transitions agree with each other, while the $V_{p,blue}$ values differ by 0.1 km s^{-1} for the two transitions, suggesting that the velocity difference should be attributed to the intrinsic property of the gas rather than uncertainties in ν_{rest}.

The three hyperfine (HF) components of the HCN (1–0) emission, showing blueskewed profiles, have comparable peak intensities, suggestive of large optical depths. We have performed hyperfine structure (HFS) analysis of the blue- and redshifted components separately assuming that infall motions traced by the blue- and redshifted emission are independent, and that each emission can be approximated by a Gaussian profile. Our analysis gave a representative LSR velocity (V_0) of $V_{0,blue}$ =−2.90 ± 0.01 km s^{-1}, intrinsic velocity width (Δv_{int}) of 0.34 ± 0.01 km s^{-1}, and total optical depth (τ_{tot}) of 15 ± 2 for the blueshifted components. Similarly, we obtained $V_{0,red}$ =−2.21 ± 0.03 km s^{-1}, Δv_{int} = 0.17 ± 0.02 km s^{-1}, and τ_{tot}= 12 ± 1.6 for the redshifted components. These τ_{tot} values lead to optical depths (τ) of 1.6 and 1.3 for the blue- and redshifted F = 0–1 components, 8.1 and 6.7 for the F = 2–1 components, and 4.9 and 4.0 for the F = 1–1 components, respectively, with an uncertainty of 20%. The estimated τ for the blue- and redshifted gas of each HF component are comparable to each other, as expected from their intensity ratios, and seem to be consistent with the fact that the absorption dips in the F = 2–1 and F = 1–1 transitions are deeper than that in the F = 0–1 transition.

Figure 2 compares total integrated intensity maps of the $H^{13}CO^+$ (1–0) (Paper I) and HCO^+ (1–0) emission. Both lines show a similar spatial structure, but the HCO^+ emission is more extended than the $H^{13}CO^+$. Figure 3 represents the HCO^+ (3–2) and (1–0) mosaic spectra taken with 30″ spacing. Here, the (1–0) spectra were produced from the smoothed cube data in the same manner as for Figure 1. Both the transitions show the blueskewed profiles not only toward the core center, but also

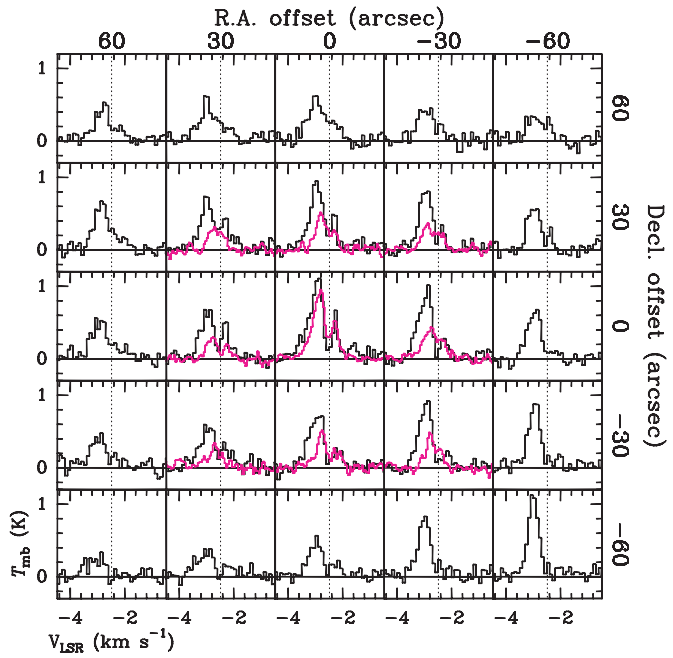

Figure 3. Mosaic spectra of the HCO^+ (1–0) (black histogram) and HCO^+ (3–2) (purple histogram) lines in main-beam temperature (T_{mb}) scale with 30″ spacing centered on the 30″ spacing grid centered at the GF 9-2 core center. The vertical dashed line in each panel indicates V_{sys}.

at some surrounding positions of, e.g., $(\Delta\alpha, \Delta\delta) = (0'', \pm 30'')$ and $(+30'', 0'')$. Due to the limited S/N, it is difficult to assess whether or not the outer spectra (e.g., in the row of $\Delta\delta = +60''$ and the column of $\Delta\alpha = +60''$) have blueskewed profiles. The HCO^+ (1–0) emission show strong blueshifted emission toward the southwest, leaving a possibility that the emission represents another blueshifted component of the gas. In fact, the possibility is supported by position–velocity (PV) diagrams of the HCO^+ (1–0) and $H^{13}CO^+$ (1–0) emission shown in Figure 4. Clearly, there exists an isolated blueshifted component of the HCO^+ emission peaked at the offset position of $\sim -120''$ (Figure 4(a)). It should be noted that the velocity structures in the central region of $r \lesssim 30''$ are fairly consistent with the blueskewed profiles expected for infall motion.

4. DISCUSSION

Although the nature of the blueshifted HCO^+ emission to the southwest is not clear, our observations show that the gas motion in the central region ($r \lesssim 30''$) is governed by the infall. Therefore, we focus on the discussion of the spectrum toward the core center. To give more quantitative constraints on the gas infall, we have developed a radiative transfer code to model the $H^{12}CO^+$ and $H^{13}CO^+$ spectra for a spherical core dominated by infall motion. The code was originally written for the CO emission from a protoplanetary disk (Omodaka et al. 1992). In this model, we assumed that local thermodynamic equilibrium (LTE) holds for the line excitation. To calculate the spectra, we assumed that the gas is infalling with a constant velocity ($v = V_{inf}$) for $r \leq 30''$, whereas a static state ($v = 0$) prevails for $30'' < r \leq 100''$ from Figures 2–4. We adopted the mass density radial profile falling between those of the LPH and Shu's solutions: $\rho(r) = 3c_{iso}^2/(2\pi G)r^{-2}$. Namely, $\rho(r) = 2.7 \times 10^{-16}(r/200\ \mathrm{AU})^{-2}$ g cm^{-3} at $T = 9.5$ K (Paper I). We used a radial temperature profile $T(r) = 1000\,(r/1\ \mathrm{AU})^{-p}$ K with $p = 1/2$, on the basis of the temperature profile at 2×10^4 yr after the formation of a protostar in Figure 2 by Masunaga & Inutsuka (2000a). We took a constant fractional abundance for $H^{13}CO^+$ of $(8.5 \pm 4.7) \times 10^{-12}$ (Paper I) all over the core, although this simplification may not be valid in a dynamically collapsing core (e.g., Aikawa et al. 2001). For a comparison with the observed spectra, we smoothed the calculated ones with a Gaussian function with $\theta_{HPBW} = 26''$ and converted the flux density into the T_{mb} (see Omodaka et al. 1992).

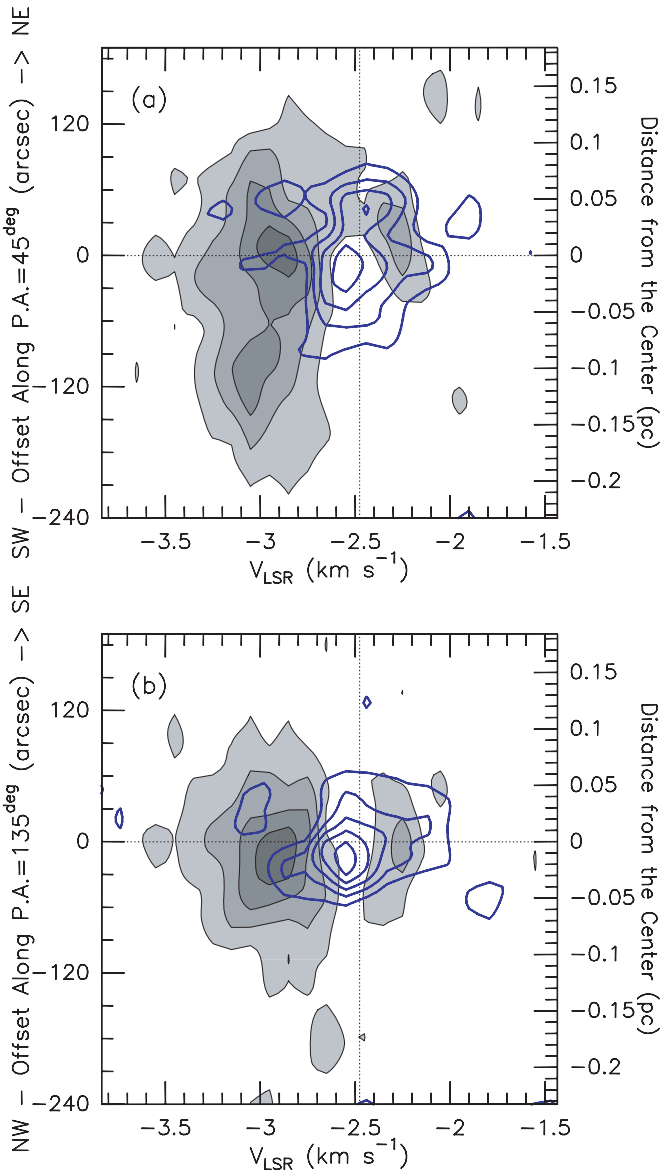

Figure 4. PV diagrams of the HCO^+ (1–0) (grayscale with thin contour; this work) and $H^{13}CO^+$ (1–0) (blue; Paper I) emission along (a) the major (P.A.= +45°) and (b) minor (P.A.= 135°) axes passing the core center. Both the line data are smoothed with the 26″ beam the same as for Figure 2. The contour levels are the 3σ interval starting from the 3σ level of each emission where $\sigma = 131$ and 57 mK per velocity channel in T_{mb} for the HCO^+ and $H^{13}CO^+$ emission, respectively. The vertical dashed line in each panel indicates V_{sys}.

Figure 5 compares calculated and observed spectral profiles whose intensity scales are normalized. Here we discuss only the velocity differences between the blue- and redshifted peaks because our calculations adopted the LTE approximation, and because rigorous calculations (Masunaga & Inutsuka 2000b) show that the intensities of the model spectra vary significantly with the evolutionary stage of the protostar. We searched

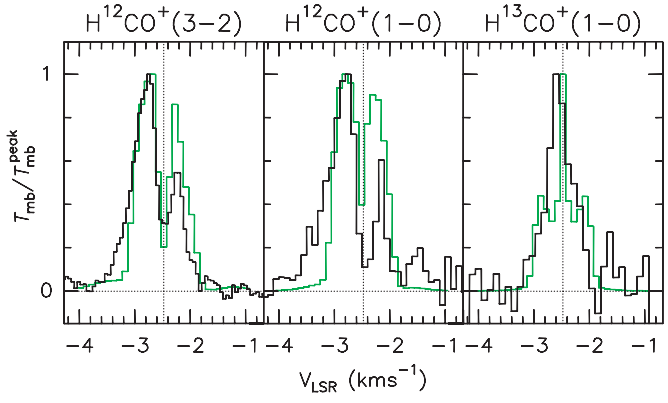

Figure 5. Model (green) and observed (black) spectra of the $H^{12}CO^+$ (3–2), $H^{12}CO^+$ (1–0), and $H^{13}CO^+$ (1–0) emission toward the center of the core. The model spectra are calculated with the most plausible infall velocity (V_{inf}) of 0.5 km s^{-1} (see the text). To compare with the observed profiles, the model spectra are convolved by a Gaussian function with $\theta_{HPBW} = 26''$ (see Section 4).

for a plausible value of V_{inf} to reproduce the observed line profiles, and found that a velocity of 0.5 km s^{-1} gives the most plausible $H^{12}CO^+$ line profiles. In fact, the calculated $H^{12}CO^+$ spectra have a consistency with the observed ones within the errors (Figure 5). We confirmed that the two cases of $V_{inf} = 0.3$ and 0.7 km s^{-1} cannot reproduce the observed velocity differences between the blue- and redshifted peaks (Section 3). Note that $V_{inf} = 0.5$ km s^{-1} agrees with an estimate from $V_{inf} \approx \frac{1}{2}|V_{blue} - V_{red}|/\cos(45^\circ) = 0.45$ km s^{-1} in Section 3. Although the model $H^{13}CO^+$ line profile has the blue and red shoulders due to the central infalling region, the overall line profile seems to agree with the observed one that has a single peak at V_{sys} owing to the outer static gas. As for p, we also tested the two cases of $p = 1/3$ and 1, but found that neither can reproduce the observed absorption features around V_{sys}. Here, the p value of 1/3 is expected in the case that the dust opacity coefficient has frequency dependence $\propto \nu^2$ (Doty & Leung 1994). We addressed such a case because the overall properties of the dust in the GF 9-2 core, which is at a very early evolutionary stage, may be similar to those for the interstellar medium. In addition, the deep absorption dips around V_{sys} require the presence of a cold static envelope surrounding the contracting region.

It is known that a density profile $\rho(r) \propto r^{-\frac{3}{2}}$ is expected for a central free-fall region onto the forming protostar. Our previous observations revealed that the profile $\rho(r) \propto r^{-2}$ continues down to the central $r \sim 600$ AU region, although it was impossible to know whether or not $\rho(r) \propto r^{-\frac{3}{2}}$ exists at $r \lesssim 600$ AU owing to our insufficient angular resolution. Given $p = 1/2$ and $V_{inf} = 0.5$ km s^{-1}, we further calculated the HCO^+ spectra for the case that the gas is freely falling onto the central protostar of 0.1 $M_\odot$ (Paper I) at $r < 600$ AU. However, the resultant line profiles were not significantly changed compared with the above results.

Although the LPH solution well describes the ongoing collapse in the GF 9-2 core (Paper I), we examined the case for Shu's solution. We assumed that the gas is freely falling toward a 0.1 $M_\odot$ protostar at $r \lesssim 600$ AU and is static at $r \gtrsim 600$ AU on the basis of the observed density profile (Paper I). The calculated HCO^+ spectra for the two transitions do not show blueskewed profiles, but double-peaked spectra having an absorption dip at the V_{sys}. This would be a natural consequence of having the compact free-fall region embedded in the large static core.

Assuming that the infall motion is radial, we can estimate the mass accretion rate $\dot{M}_{acc}$ as $4\pi r^2 \rho V_{inf}$. We obtain $\dot{M}_{acc}$ of 2.5×10^{-5} $M_\odot$ yr^{-1} with uncertainty of a factor $\sim$ 2. Since theoretical models of protostar formation (e.g., Stahler et al. 1980; Masunaga & Inutsuka 2000a) predict that the protostar radius, R_*, should be $\sim$ 5 $R_\odot$ for a low-mass protostar, we can calculate an accretion luminosity (L_{acc}) for the central protostar(s) of $L_{acc} = 16\ L_\odot\ G(M_*/0.1\ M_\odot)[\dot{M}_{acc}/(2.5 \times 10^{-5}\ M_\odot\ \mathrm{yr}^{-1})](R_*/5\ R_\odot)^{-1}$. This seems reasonable compared with the luminosity expected for a protostar at a very early evolutionary stage (see, e.g., Figure 7 in Masunaga & Inutsuka 2000a). Consequently, our study confirms that the gas in the GF 9-2 core is infalling onto the protostar(s) in the central region, and that the infalling velocity is consistent with the prediction from the LPH solution. Furthermore, we plan to perform deeper integration of these HCO^+ lines to examine the presence of the infalling gas in the outer region of the core.

R.S.F. gratefully acknowledges Thomas A. Bell, Thomas G. Phillips, and Ruisheng Peng for their generous help during the CSO observations. The authors sincerely thank Thomas A. Bell for a critical reading of the manuscript at the final stage of preparation. This work is partially supported by Grant-in-Aids from the Ministry of Education, Culture, Sports, Science and Technology of Japan (No. 19204020 and No. 20740113).

Facilities: Nobeyama 45 m telescope, Caltech Submillimeter Observatory 10.4 m telescope

REFERENCES

Aikawa, Y., Ohashi, N., Inutsuka, S.-I., Herbst, E., & Takakuwa, S. 2001, ApJ, 552, 639
Doty, S. D., & Leung, C. M. 1994, ApJ, 424, 729
Furuya, R. S., Kitamura, Y., & Shinnaga, H. 2006, ApJ, 653, 1369 (Paper I)
Furuya, R. S., Kitamura, Y., & Shinnaga, H. 2008, PASJ, 60, 421
Hunter, C. 1977, ApJ, 218, 834
Larson, R. B. 1969, MNRAS, 145, 271
Looney, L. W., Mundy, L. G., & Welch, W. J. 2003, ApJ, 592, 255
Mardones, D., Myers, P. C., Tafalla, M., Wilner, D. J., Bachiller, R., & Garay, G. 1997, ApJ, 489, 719
Masunaga, H., & Inutsuka, S.-I. 2000a, ApJ, 531, 350
Masunaga, H., & Inutsuka, S.-I. 2000b, ApJ, 536, 406
McKee, C. F., & Ostriker, E. C. 2007, ARA&A, 45, 565
Myers, P. C., Mardones, D., Tafalla, M., Williams, J. P., & Wilner, D. J. 1996, ApJ, 465, L133
Omodaka, T., Kitamura, Y., & Kawazoe, E. 1992, ApJ, 396, L87
Onishi, T., Mizuno, A., & Fukui, Y. 1999, PASJ, 51, 257
Penston, M. V. 1969, MNRAS, 144, 425
Remijan, A. J., & Hollis, J. M. 2006, ApJ, 640, 842
Sawada, T., et al. 2008, PASJ, 60, 445
Shu, F. H. 1977, ApJ, 214, 488
Stahler, S. W., Shu, F. H., & Taam, R. E. 1980, ApJ, 241, 637
Walker, C. K., Lada, C. J., Young, E. T., Maloney, P. R., & Wilking, B. A. 1986, ApJ, 309, L47
Ward-Thompson, D., Buckley, H. D., Greaves, J. S., Holland, W. S., & André, P. 1996, MNRAS, 281, L53
Ward-Thompson, D., Scott, P. F., Hills, R. E., & Andre, P. 1994, MNRAS, 268, 276
Zhou, S., Evans, N. J. II, Koempe, C., & Walmsley, C. M. 1993, ApJ, 404, 232